Observations of Turbulence in Stratified Flow

L. MAHRT AND N. GAMAGE

Department of Atmospheric Sciences, Oregon State University, Corvallis, OR 97331

(Manuscript received 5 May 1986, in final form 28 October 1986)

ABSTRACT

Various theoretical properties of the structure function are evaluated. Additional functions are constructed to describe the overall influence of stratification, the anisotropy and intermittency of the turbulence, and the asymmetry of the main drafts.

These functions and the usual spectral decomposition are computed from aircraft-measured turbulence data collected in nocturnal boundary layers and in turbulence over mountainous terrain. Certain features of the turbulence are found to depend more on stability than on the external situation. Three general types of turbulence are found: 1) intermittent turbulence driven by shear-driven overturning; 2) continuous turbulence where strong drafts in the presence of shear are characterized by sharp boundaries or microfronts, particularly on their upstream sides; and 3) weaker continuous turbulence. The costructure fields are generally consistent with vertical gradient transfer. However, the bora turbulence on larger scales is dominated by horizontal motions perpendicular to the mean shear.

1. Introduction

In stratified geophysical flows, turbulence often coexists with gravity waves and two-dimensional horizontal motions and is difficult to isolate with actual data. Gravity wave motions can initiate turbulence through intensification of local shear while turbulent motions are also thought to initiate gravity waves (Finnigan et al., 1984; Townsend, 1968) as well as to decay to relatively large horizontal motions. The latter are sometimes referred to as vortical modes, fossil turbulence or two-dimensional turbulence. The initiation of gravity waves and decay to two-dimensional turbulence generally corresponds to energy transfer to larger scales while the generation of turbulence by larger-scale shear and subsequent formation of an inertial subrange corresponds to energy cascade to smaller scales.

In the inertial subrange, energy is transferred to smaller scales through vortex stretching and shear instabilities at sequentially smaller scales. The signature for the inertial subrange is the $-5/3$ power dependence of spectral energy on wavenumber. However, larger scale horizontal motions greater than a few kilometers also seem to exhibit an approximate $-5/3$ dependence on wave number (Lilly, 1983). At these scales, the energy transfer is thought to occur from smaller- to larger-scale motions.

The intermediate scales, between a few kilometers and the smaller scales containing the inertial subrange, include the shear generated eddies, or "energy containing eddies", and often include gravity waves as well. A broad peak of spectral energy may occur associated with the energy containing turbulent eddies while peaks at larger scales can occur associated with gravity waves. However, such energy maxima are often not well defined or are missing. In fact, Weinstock (1980) proposes a minimum of spectral energy at the generation scale. With this proposition, energy is transferred from the generation scale to both smaller and larger scales.

In this study, we will examine certain statistical features of turbulence in a few atmospheric flows characterized by a range of strengths of stratification. Certain structure functions will be constructed to emphasize various impacts of the stratification on the turbulence. We will analyze fast-response data collected by the NCAR Queen Air in the nocturnal surface inversion layer during synoptically quiet periods of the Severe Environmental Storms and Mesoscale Experiment (SESAME). We also analyze data in the bora of 6 March 1982 observed with NCAR Electra as part of the Alpine Experiment (ALPEX). Much of the data will be presented in terms of the structure function which is discussed in section 2. Flow characteristics are studied in terms of spectral decomposition and the structure functions in section 3. Variation of turbulence characteristics within the bora and nocturnal boundary layers are revealed by evaluation of certain physically motivated functions of the structure and their dependence on stability (section 4). Characteristics are interpreted in terms of simple features of the dominant eddies in section 5. The nature of the covariance fields and the relationship between the velocity structure and shear are explored in section 6.

2. Statistical techniques

In this section we mathematically analyze the statistical tools which will be applied in subsequent sec-

tions. Consider generic variables ϕ and ψ decomposed as

$$\phi = \bar{\phi} + \phi' \tag{1}$$

$$\psi = \bar{\psi} + \psi' \tag{2}$$

where ϕ' and ψ' are ideally intended to represent turbulent fluctuations although complete physical decomposition is not usually possible. Generally, the overbar operator is chosen more pragmatically to filter out trend and larger-scale motions which are observed with inadequate sampling.

We then define the lagged covariance function,

$$\beta_{\phi\psi} = [\phi'(x+r)\psi'(x)], \tag{3}$$

where r is the lag or separation distance which can be a vector quantity. The averaging operator [ ] will usually represent simple unweighted averaging, although it could also be chosen to be the same averaging operator as the overbar. In studies of turbulence, (3) is usually referred to as the correlation function even though the true correlation function would require dividing (3) by the standard deviations for ϕ and ψ and thus be equal to

$$[\phi'(x+r)\psi'(x)]/([\phi'(x)^2]^{1/2}[\psi'(x)^2]^{1/2}).$$

The cross spectral energy is defined in terms of the Fourier transform of the covariance function (3). If ψ and ϕ are the same variable, then the autocorrelation function and spectral energy are recovered.

Of considerable use to this study will be the co-structure function defined as

$$D_{\phi\psi}{}^n(r) = [\langle\{\phi(x+r) - \phi(x)\}\{\psi(x+r) - \psi(x)\}\rangle^{n/2}]. \tag{4}$$

We will study primarily the case ($n = 2$) which will be symbolized simply as $D_{\phi\psi}(r)$. If ϕ and ψ are the same variable, then (4) with $n = 2$ becomes the second moment or the structure function. Some use will also be made for the third (skewness) and fourth (kurtosis) moments.

The structure function has found useful application to turbulence (e.g., Monin and Yaglom, 1975; Antonia and Van Atta, 1975, 1978; Orszag, 1977; Panofsky and Dutton, 1984) and was employed in the original development of the theory of the inertial subrange (Kolmogorov, 1941) modified in Kolmogorov (1962). We will now examine some properties of the structure function relative to this study and examine the relationship between the structure function, covariance function, and spectral decomposition.

Consider the special case of a single variable with the mean removed which is homogeneous (or stationary) so that

$$[\phi(x+r)\phi(x+r)] = [\phi(x)\phi(x)].$$

Then substituting the resulting expression for the autocorrelation function (3) into the definition of the structure function (4), we find that the structure function and autocorrelation function are related through the expression (Monin and Yaglom, 1975)

$$D_{\phi\phi}(r) = 2B_{\phi\phi}(0)\{1 - B_{\phi\phi}(r)/B_{\phi\phi}(0)\}. \tag{5}$$

Since the magnitude of the correlation function is constrained to be less than unity, i.e.,

$$-1 \leq B_{\phi\phi}(r)/B_{\phi\phi}(0) \leq 1, \tag{6}$$

the magnitude of the structure function for stationary records is constrained by the limits

$$0 \leq D_{\phi\phi}(r) \leq 4B_{\phi\phi}(0). \tag{7}$$

Since the covariance function of a stationary record approaches zero for large separation distances, relationship (5) implies that

$$D_{\phi\phi}(r) \to 2B_{\phi\phi}(0); \quad r \to \text{large}. \tag{8}$$

Breaking the change of ϕ over separation distance r into incremental changes over the minimum spatial increment $r_{\min}$ (resolution), substituting this sum into the definition of the structure function (4), and using Schwarz's inequality, it follows (Monin and Yaglom, 1975) that the rate of increase of the structure function with increasing separation distance is bounded by the relationship

$$D_{\phi\phi}(r) \leq (D_{\phi\phi}(r_{\min})/(r_{\min})^2)r^2. \tag{9}$$

Since $r_{\min}$ is fixed, the structure function can increase no faster than a quadratic dependence on lag. This particular relationship (9) does not require the assumption of stationarity.

To study the difference between the way in which the structure function and spectra decompose the motion, it is useful to consult the following relationship for stationary flow which is obtained by substituting the Fourier transform of (3) into (5) (Monin and Yaglom, 1975; Babiano et al., 1985):

$$D_{\phi\phi}(r) = 2\int_k (1 - \cos kr)E_{\phi\phi}(k)dk \tag{10}$$

where $E(k)$ is the one-dimensional spectral energy density at wavenumber k. This relationship shows that a wave mode which is sharply represented in Fourier space by a single wavenumber is spread over a range of separation distances when represented by the structure function (Fig. 1).

On the other hand, the scale of motions with sharp horizontal boundaries, such as a series of top hat profiles, is clearly identified by the structure function but becomes somewhat fuzzy with spectral representation (Fig. 1). It will be found that the main turbulent drafts are often characterized by sharp horizontal boundaries. Of course, the total turbulence field is much more complicated than top hat functions and significant variance is found at all wavenumbers and separation distances.

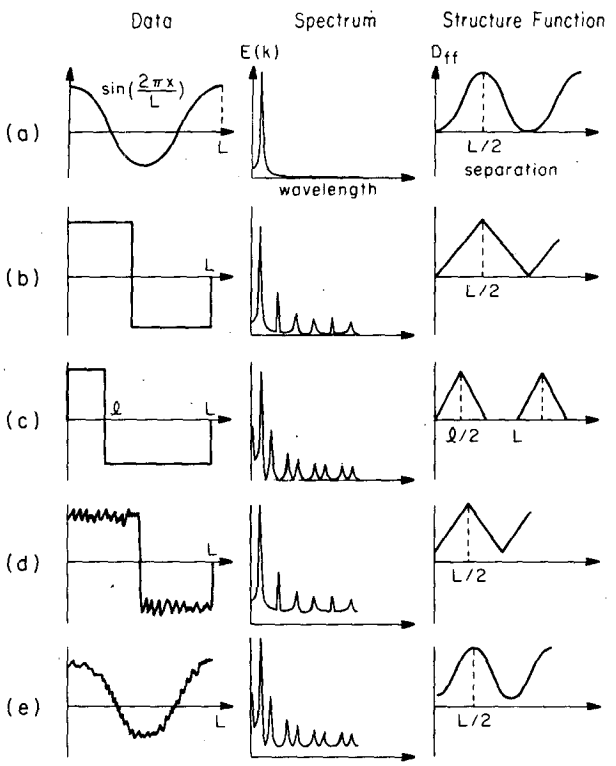

FIG. 1. Spectral density (middle column) and structure functions (right) for artificial records (left) with a record length of 10 cycles. The artificial functions are (a) sinusoidal, (b) top hat (square wave), (c) top hat with unequal spacing, (d) square wave with added white noise and (e) sinusoidal function with added white noise. The spectra were computed without padding, tapering or smoothing. The principal spectral peak occurs at wavenumber $2\pi/L$.

Some of the aforementioned relationships can be extended to include cospectra and costructure. For example, we will make use of the relationship (Monin and Yaglom, 1975):

$$D_{\phi\psi}(r) = 2\int_k (1-\cos kr)E_{\phi\psi}(k)dk \qquad (11)$$

where $E_{\phi\psi}(r)$ is the cross spectrum of ϕ and ψ. Note that the costructure captures the magnitude of the phase difference but not the sign.

The above interrelationships apply only to stationary (homogeneous) records. The spectrum and covariance function are not uniquely related to the structure function for nonstationary records. Since geophysical turbulence is usually quite nonstationary and inhomogeneous, even to a first approximation, the relationship between the spectrum and the structure function is not predictable.

Therefore, it is important to assess the influence of trend on spectra and the structure function. Lumley and Panofsky (1964) show that the structure function is less sensitive to linear trend than the covariance function. Here we consider a somewhat more general function for the trend which consists of linear trend and a limited number of simple wave modes:

$$F(x) = ax + \sum_i b_i \sin k_i x.$$

This large scale motion $F(x)$ is superimposed upon the smaller-scale turbulence $f(x)$. To simplify the analysis, we will assume that $f(x)$ and $F(x)$ are uncorrelated and that the linear trend and the individual wave modes are also uncorrelated with each other. These conditions are satisfied if the turbulence is stationary and the record is long compared to the largest wave length.

Then the total covariance function is

$$\beta(r) = \beta_f(r) + \frac{1}{L}\int_{-L/2}^{L/2} a^2 x(x+r)dx + \sum_i \frac{1}{L}\int_{-L/2}^{L/2} b_i^2 \sin k_i x \sin k_i(x+r)dx \qquad (12)$$

where $\beta_f(r)$ is the covariance due to the turbulence.

Using the approximation for the lagged correlation function of a sine curve for large $k_i L$,

$$\int_{-L/2}^{L/2} \sin k_i x \sin k_i(x+r)dx \Big/ \int_{-L/2}^{L/2} \sin^2 k_i x dx \approx \cos k_i r, \qquad (13)$$

we obtain after integrating (12)

$$\left.\begin{aligned} \beta(r) &= \beta_f(r) + a^2L^2/12 + \sum_i h_i(L) b_i^2 \cos k_i r \\ h_i(L) &= \frac{1}{L}\int_{-L/2}^{L/2} \sin^2 k_i x dx \end{aligned}\right\}. \qquad (14)$$

Note that $h_i(L)$ is bounded by ½. The corresponding structure function is

$$D(r) = D_f(r) + \frac{1}{L}\int_{-L/2}^{L/2} \{a(x+r) - ax\}^2 dx + \sum_i \frac{1}{L}\int_{-L/2}^{L/2} \{b \sin k_i(x+r) - b \sin k_i x\}^2 dx. \qquad (15)$$

Using the trigometric identity (13), we obtain

$$D(r) = D_f(r) + a^2r^2 + 4\sum_i h_i(L) b_i^2 \sin^2\left(\frac{k_i r}{2}\right). \qquad (16)$$

First consider the error due to the influence of linear trend. For the structure function, this error vanishes with vanishing separation distance (16) but is independent of separation distance for the covariance function (14). The ratio of this error for structure function to that of the covariance function is

$$12r^2/L^2. \qquad (17)$$

Since r should be less than $O(0.1)L$ to control the influence of sampling problems on $f(x)$, the error for the structure function will always be at least one order of

magnitude smaller than the corresponding error for the covariance function. The errors due to the wave modes are of the same order of magnitude for both structure and covariance functions but depend on the separation distance.

Of more importance is the relative size of the trend-related errors with respect to the magnitude of the structure and covariance functions. Percentage errors can be estimated by specifying the form of the covariance function for the turbulence, and using relationship (5) between the structure and covariance functions for the homogeneous part of the flow $\beta_f(r)$.

If we assume $\beta_f(r) = \beta_f(0)g(r)$, then the relative error for the covariance function is

$$\sum_i h_i(L)b_i^2 \cos k_i r/\{\beta_f(0)g(r)\} \tag{18}$$

and the error for the structure function is

$$2\sum_i h_i(L)b_i^2 \sin^2(k_i r/2)\{(1-g(r))\beta_f(0)\}. \tag{19}$$

As an example, the dependence of the relative errors on scale for

$$g(r) = e^{-mr} \tag{20}$$

for a single wave mode is plotted in Fig. 2 for three different values of m. We see that the relative errors for the structure function are smaller at small scales for the various values of m. Similar results were obtained for more sophisticated correlation functions such as parabolic decay where characteristic negative correlations appear at larger separation distances.

Therefore, at small scales, the structure function appears to be less vulnerable to trend than the covariance function. Detrending and filtering for application of the structure function to the present data were found to be unnecessary which eliminates the sensitivity to the somewhat arbitrary choice of the filter cutoff value or detrending procedure. From a more general point of view, the structure function does not require determination of a mean, an ambiguous process when motions occur on a variety of scales.

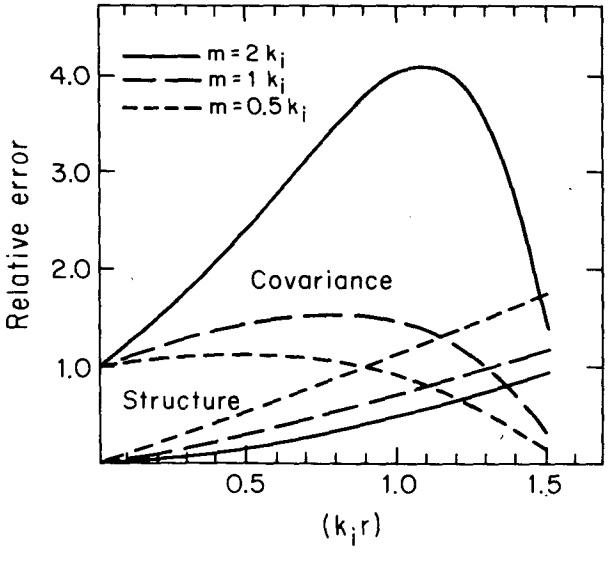

FIG. 2. Relative errors due to periodic trend for the covariance (upper curves) and structure functions (lower curves) for turbulence correlation function [Eq. (20)].

Furthermore, the structure function is generally smooth and stable (Babiano et al., 1985) and does not require extra smoothing or adjustments of band width as sometimes occurs with spectra and often occurs with cospectral decomposition. On the other hand, spectral decomposition is orthogonal and allows direct comparison with many previous theoretical developments and observational studies. Furthermore, cospectral decomposition determines the phase between two variables. In other terms, the spectral decomposition potentially contains more information, but is more vulnerable to various sampling problems. In the following analysis, both structure and spectral functions will be computed for completeness. The spectra and structure functions lead to similar qualitative conclusions, although cospectra were noisy and required substantial smoothing.

3. Flow situations

The aircraft instrumentation used in SESAME and ALPEX is similar to that discussed in Wyngaard et al. (1978) except that for the ALPEX data, correction for thermal inertia of the thermistor housing was not necessary due to improved instrumentation. In ALPEX, five flight legs were flown in and above a bora event over the coastal range of northern Yugoslavia on 6 March 1982, each at a different elevation using the NCAR Electra. The flight paths of interest are located on a line between Zagreb, Senj, and Losinj. The flight levels and approximate surface terrain are shown in Fig. 3. Turbulence immediately downstream (southwest) of the crest of the coastal range is quite strong. Here "downstream" is in reference to the bora flow from the northeast which is directed roughly parallel to the aircraft flight and perpendicular to the coastal range. The bora occupies the two lowest flight levels upstream and over the mountain range and then descends rapidly downstream from the mountain range. Flow from the southeast and roughly parallel to the coastal range dominates above the bora and is important in the turbulence region downstream from the mountain range. For convenience, we will loosely refer to the entire flow as the bora when comparing with nocturnal boundary-layer cases.

The turbulence extends to the surface downstream from the mountain range so that this part of the bora can be considered as a boundary layer flow. Heating occurs at the surface and some cloudiness occurs aloft but both appear to have little influence on turbulence

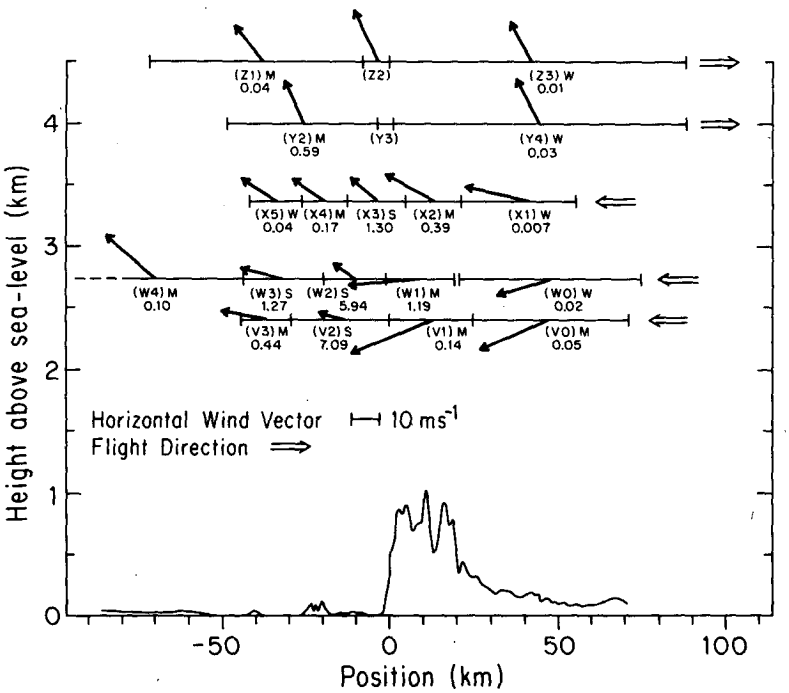

FIG. 3. Cross section of aircraft flights. The cross section faces northwestward with northeastward to the right. Double arrows in the right-hand margin indicate flight direction. Record segments are labeled for future reference. Shown are values of the structure function for vertical velocity at 200 m separation distance. Segments with no structure function values were considered too short for statistical reliability. The record segments are divided into classes of strong turbulence (S), moderate turbulence (M), and weak turbulence (W). Solid arrows indicate averaged horizontal wind vectors plotted in a local planview coordinate with north directed toward the top of the figure.

at the levels of aircraft observations where the bulk shear appears to be quite large and the heat flux is downward.

In the region of strongest turbulence, sharp differences of vertical motion in excess of 10 m s^{-1} over horizontal distances of a few tens of meters are common, which are much stronger shears than in usual boundary layer turbulence. Figure 4 shows the vertical velocity record for the section of strongest turbulence at the lowest flight level. Subregions of turbulence of different intensities and characteristics were usually well defined. This allowed partitioning of the flight legs into sections which are noted in Fig. 3. Based on the numerical value of the small-scale vertical velocity variance, the various sections of turbulence were nominally classified according to the occurrence of strong, moderate or weak turbulence. For example, the standard deviation of the linearly detrended, 1 km high pass vertical velocity is roughly 1 m s^{-1} for records in the strong class, a few tens of centimeters per second for the moderate class and 5–10 cm s^{-1} for the weak class.

The bora features will be compared with features deduced from aircraft measurements collected by the NCAR Queen Air in two nocturnal boundary layer flows observed during SESAME. In the nocturnal boundary layer flow observed early in the morning of 5 May 1979, intermittent turbulence is observed at the top of a nocturnal surface-based inversion about 50 m thick (Mahrt, 1985). This turbulence is generated by shear between weak downslope surface flow from the northwest and overlying weak ambient flow from the south. The turbulence in the bulk of the surface inversion layer is very weak or nonexistent. The intermittent turbulence at the top of the inversion layer was observed with six horizontal aircraft legs of approximately 15 km length and oriented in the north–south direction. Statistics will be computed for each leg. We will loosely refer to these six legs as the nocturnal boundary-layer class of weak turbulence even though continuous turbulence was not maintained. For these legs, the standard deviation of the linearly detrended 500 m high pass vertical velocity is typically 5 cm s^{-1} although vertical velocity fluctuations within turbulent patches are often several factors greater.

The turbulence in the second nocturnal boundary layer, observed early in the morning of 6 May, is much stronger. Here ambient winds of nearly 20 m s^{-1} generate stronger boundary-layer turbulence several hundred meters deep. However, significant surface cooling maintains some stable stratification across the boundary layer. This boundary layer was observed in five horizontal aircraft legs again oriented in the north-

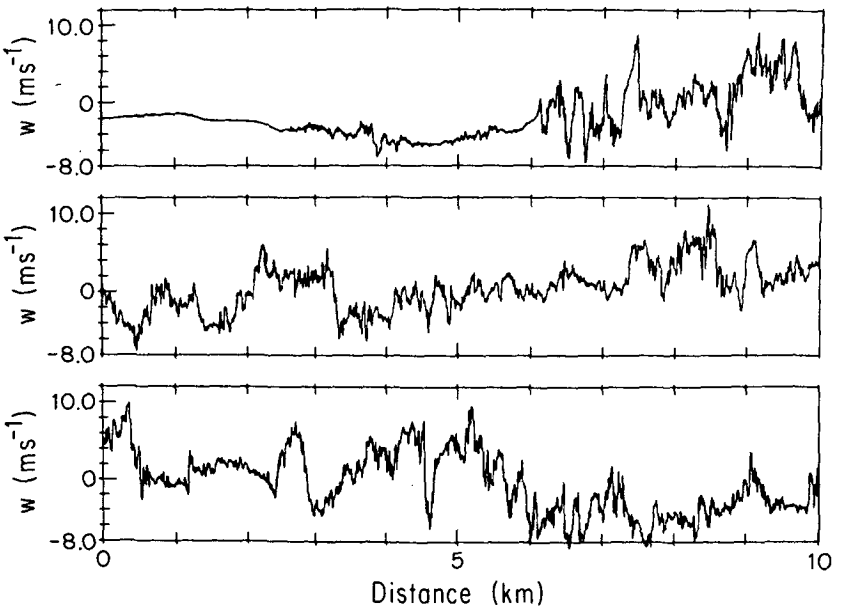

FIG. 4. Example of the record for vertical velocity in the bora.

south direction with a length of about 15 km. Shear occurs throughout the boundary layer and is generally directed toward the northeast. Statistics will be computed for each leg which will comprise the nocturnal boundary-layer class of strong turbulence. The strength of the turbulence in this class is intermediate between the bora classes of strong and moderate turbulence. For the various legs, the standard deviation of the linearly detrended 500 m high-pass vertical velocity is typically 50 cm s^{-1}.

The classes of turbulence strength can also be considered as stability classes. The strong turbulence exhibits only secondary influences of the stratification while the weak turbulence is significantly suppressed by the stratification. To reduce sampling problems, various statistics will be composited for each of the five classes of records.

4. Dependence on stability and scale

In this section, we study the dependence of statistical properties of the observed turbulence on stability and horizontal scale. This is done by examining the spectra and various structure functions.

a. Spectra and structure functions

The composited energy spectral density and structure functions are plotted in Fig. 5. The u-component is directed along the flight path. Calculations were carried out for scales up to $\frac{1}{10}$ of the record length; larger scales would be observed with sampling problems. While the structure functions are thought to be less sensitive to trend (section 2), most of the general features of the structure function are predicted by the energy spectra. When comparing the two types of calculations, one must note that the variance for the structure function is realized at scales which are smaller than those for the spectra, since the structure function is based on gradients while the spectrum responds to complete cycles. For example, with a periodic function, the predominant scale is a factor of 2 smaller in the structure function as compared to the spectrum. With up- and downdrafts, the structure function responds more to the scale of the narrow boundaries of sharp gradients than does the spectrum (see section 2).

At the smallest scales, the spectrum and structure function are generally characterized by constant slope (Figs. 5, 9). For the class of strongest bora turbulence, the slopes of the composite spectral density and structure function are both well approximated by inertial subrange relationship corresponding to a $-\frac{2}{3}$ slope for the spectral coordinates in Fig. 5 and $+\frac{2}{3}$ for the structure function.[1] The $-\frac{2}{3}$ relationship is a good approximation for the spectral decomposition of vertical motion extending to scales of about 1 km. The structure function for vertical motion begins to increase more slowly than the $+\frac{2}{3}$ prediction for scales greater than 100 m. This decrease is not as strong for horizontal

[1] Note that the spectra at the very smallest resolvable scales are steeper than the inertial subrange prediction. The estimation of the dissipation from the inertial subrange relationship (e.g., Tennekes and Lumley, 1972, Eq. 8.3.12) indicates that the Kolmogorov scale and dissipation range are at scales much smaller than resolved here so that the steepening observed here might be due to the loss of high-wavenumber energy associated with the finite instrument response time. The isolated spectral peak at small wave numbers may result from vibration problems.

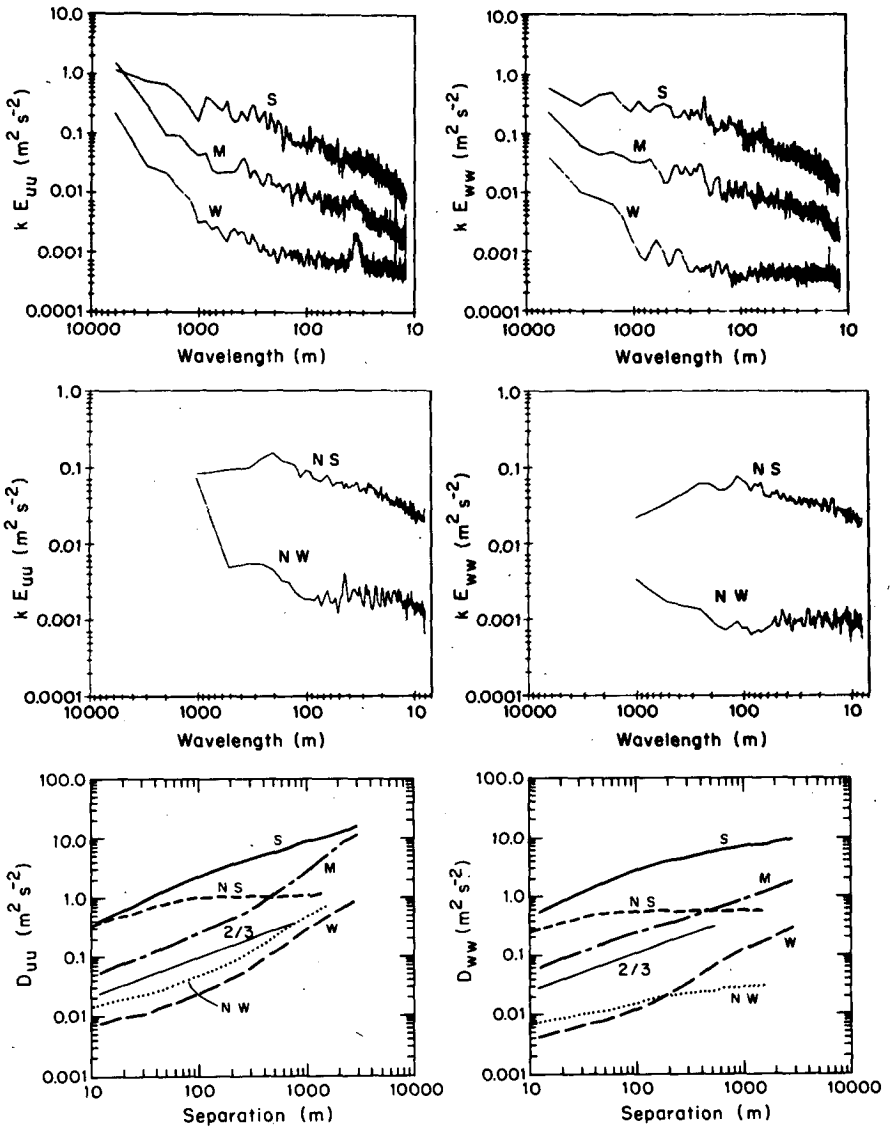

FIG. 5. Composited spectral density and structure functions for vertical motion and the horizontal velocity component in the flight direction for records in the ALPEX bora with strong turbulence (S), moderate turbulence (M), and weak turbulence (W), and for the SESAME nocturnal boundary layer case of weak turbulence (NW) and strong turbulence (NS).

velocity components suggesting some influence of stratification.

At the smallest scales for the classes of weak turbulence, the spectra for vertical motion are almost flat while the corresponding structure slopes are significantly smaller than the ⅔ value. The slopes for the horizontal velocity components are also significantly reduced by the stratification but to a lesser degree compared to the vertical motion.[2]

For convenience of reference we will casually refer to this range of small scales, with reduced slopes of the spectra and structure functions, as the buoyancy-inertial subrange although the physics of the slope reduction and its relation to various definitions of the

[2] Interpretation of spectra for the weak turbulence case is complicated by the occurrence of nonturbulent regions embedded within the intermittent turbulence. The measured vertical velocity fluctuations in the "nonturbulent" regions are on the order of a few centimeters per second and may be too weak for accurate measurement. In the turbulent regions, the vertical velocity fluctuations are on the order of tens of centimeters per second and well within the instrumental capability. Intermittency influences the slopes of the structure functions and spectra in a fundamental way (Antonia and Van Atta, 1978; Van Atta, 1971; Yaglom, 1966), although the presentation is complicated by the interplay of mean shear and stratification.

buoyancy subrange (e.g., Weinstock, 1980) are not known. It may be that the inertial subrange is shifted to smaller scales than can be adequately resolved. The implied suppression of energy at scales of a few hundred meters compared to the extrapolation from smaller scales using inertial subrange theory, (flattening of the spectra), might be due to loss of kinetic energy to potential energy. This loss would probably involve generation of gravity waves which propagate out of the region. It is also possible that the region of suppressed energy suffers from spectral energy divergence (e.g., Weinstock, 1980) where kinetic energy at slightly smaller scales cascades to smaller dissipative scales and kinetic energy at slightly larger scales participates in upscale energy transport.

We now examine somewhat larger scales—greater than one or two hundred meters—where the slopes for the spectra and structure functions change from their near constant value at smaller scales. For convenience, we will refer to these scales as the intermediate scales (see Figure 9). Such scales are expected to include the energy-containing turbulent eddies but also probably include wave motions and some influences of larger scales. We will loosely refer to the largest scales, say greater than a few kilometers, as mesoscale motions.

The difference between mesoscale and turbulent scale energies can increase the magnitudes of the slopes of the spectra at intermediate scales. That is, the slopes at intermediate scales might represent more the difference between relative strengths of the smaller-scale turbulence and mesoscale motions than the nature of the actual motions at the intermediate scales. This dependence appears in the spectral examples of Vinnichenko (1970). As a possible result, the intermediate-scale slopes for vertical motion in the bora flow are generally larger than those of the nocturnal boundary layer flows. Large variance at scales greater than a few kilometers result from strong horizontal variations of the bora. This activity is particularly intense in the bora region above the mountain ridge. Compare, for example, the structure function of vertical motion for segment W1 located above the mountain range with W3 located farther downstream (Figure 6).

For both the bora flow and nocturnal boundary layer flow, the intermediate scale slopes are greatest for the classes of weakest turbulence. With weak turbulence, greater slope at intermediate scales is required to "bridge" the turbulence and larger-scale variances. For some records of weak and even moderate turbulence, the steepening is quite sharp (Fig. 6). Since the steepening occurs at somewhat different scales for different records, it is smooth and less distinct in the composited structure function.

For classes of weakest turbulence, one could also argue that the internal gravity wave motions associated with the stronger stratification lead to greater slopes at larger scales; with saturated wave activity, a -3 spectral

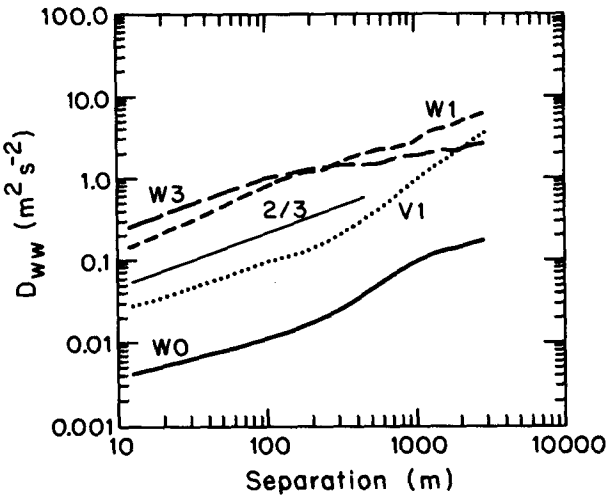

FIG. 6. The structure function for vertical velocity for individual records in the ALPEX bora flow.

slope (-2 in Fig. 5) is expected from the theory of Shur (1962) and Lumley (1964). This value roughly approximates the spectral slopes at low wave numbers for the class of weak bora turbulence.

In contrast to the classes of weak turbulence, the slopes of the structure functions at the largest scales decrease with increasing horizontal scale in the classes of strongest turbulence in the bora and in the nocturnal boundary layer. In fact for the nocturnal boundary layer class of strongest turbulence where the strength of the turbulence is greatest relative to the mesoscale energy, the slopes of the structure functions become small and the spectral slopes reverse sign for horizontal scales greater than a few hundred meters.

b. *Stability and aspect ratio*

Certain functions of the spectra and structure function reveal useful information about the nature of the turbulence. Here we will consult characteristics based on the structure function which are smoother and easier to interpret than those of the spectra at least for the present data. The results appear to be similar to those of spectral functions except for the scale shift.

The ratio $l \approx \sigma_w/N$ is often used to estimate the vertical length scale of the turbulence and to indicate the degree of suppression of vertical motions by the stratification where σ_w is the standard deviation of the vertical velocity fluctuations. Unfortunately, the Brunt-Väisälä frequency, N, often depends significantly on the vertical scale used to compute the vertical gradients. With aircraft data, the vertical gradients are contaminated by nonstationarity. The difference between the times of adjacent flight levels was 1–2 h for some of the flight legs analyzed here. Furthermore, the standard deviation of the vertical velocity, σ_w, is usually sensitive

to the choice of length scale or time scale used in the computation.

Alternatively, the vertical length scale of the turbulence can be related to the stability in terms of the buoyancy length or vertical length scale computed from the structure functions. We assume that the temperature fluctuations, and therefore fluctuation temperature gradients, are due to vertical velocity fluctuations in the presence of the stratification. We then define the buoyancy length

$$d(r) \equiv \{D_{ww}(r)\} \Big/ \left\{\frac{g}{\theta_0}\{D_{\theta\theta}(r)\}^{1/2}\right\} \qquad (21)$$

which can be written in nondimensional form as

$$\mathrm{Fr} \equiv \{D_{ww}(r)\} \Big/ \left\{r\frac{g}{\theta_0}D_{\theta\theta}(r)^{1/2}\right\}. \qquad (22)$$

This buoyancy length does not require computation of vertical gradients. On the other hand, the precise value of the above buoyancy length has less meaning in cases of mixed regions of stable and unstable stratification. With stable stratification the buoyancy length is inversely related to the influence of the stratification; i.e., with strong stratification, modest vertical motions produce large temperature fluctuations. Considering the temperature and velocity scales to be the square roots of their respective structure functions, the nondimensional ratio (22) indicates the general magnitude of the kinetic energy of vertical motion fluctuations relative to the potential energy fluctuations. In this regard, (22) is a form of the fluctuation Froude number or stability parameter where r is the length scale.

At the smallest scales, usually less than 100 m, the buoyancy length increases rapidly with horizontal scale (Fig. 7a). The rate of increase is less than linear, corresponding to slowly decreasing Froude number and thus increasing influence of stability even if small. The buoyancy length generally varies much more slowly on somewhat larger horizontal scales. This constancy corresponds to a decrease of the Froude number with increasing horizontal scale ($\sim 1/r$) implying a significant increase of stability influence with horizontal scale.

The region of slowly varying buoyancy length begins at the largest scales within the buoyancy-inertial subrange and extends to the largest scales sampled. The buoyancy length thus provides a useful index for classification of the stability of the turbulence in that the value of the buoyancy length is not sensitive to choice of scale. The values of the buoyancy length for records within each bora class showed almost no overlap with values of segments from other classes. Therefore, within the ability of this study to delineate turbulence properties, the overall stability and the strength of the turbulence are closely related and the class divisions based on turbulence strength can also be considered as stability classes.

For a fixed horizontal scale, the buoyancy length also showed correlation with estimates of $l \approx \sigma_w/N$

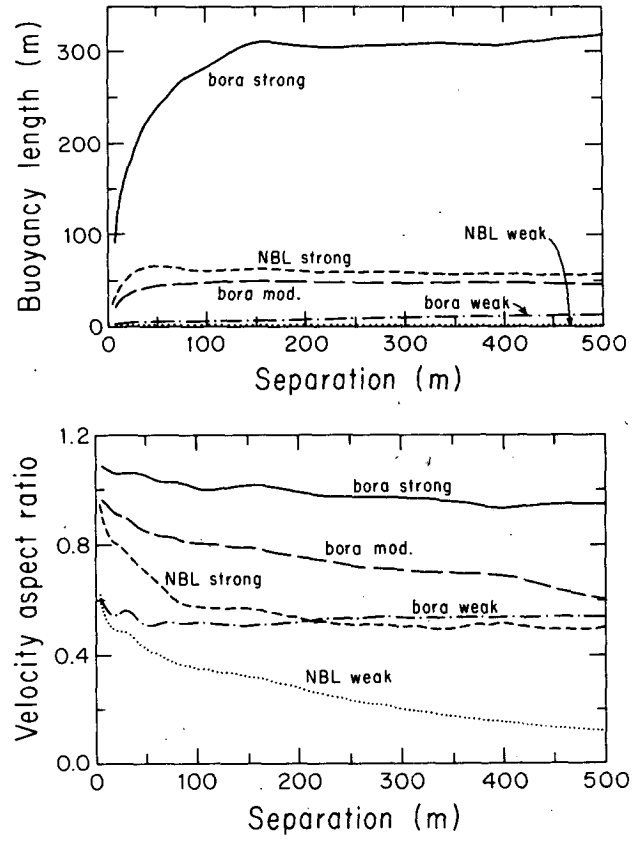

FIG. 7. (a) Composited buoyancy length (21) for records in the ALPEX bora. (b) Composited velocity aspect ratio (23) for same records.

and was characterized by comparable magnitude within the substantial uncertainties of such calculations. An analogous buoyancy length can be computed from spectral amplitudes as

$$d(k) = E_{ww}(k) \Big/ \left\{\frac{g}{\theta_0}\{E_{\theta\theta}(k)\}^{1/2}\right\}.$$

The result is somewhat noisy but exhibits the property of rapid increase at the smallest scales and generally slower variation at larger scales analogous to the behavior of $d(r)$.

The suppression of vertical motion by the stratification causes the ratio of the kinetic energy of the vertical and horizontal velocity fluctuations,

$$A(r) = D_{ww}(r) \Big/ \left\{\frac{1}{2}\{D_{uu}(r) + D_{vv}(r)\}\right\}, \qquad (23)$$

to decrease rapidly with increasing scale (Fig. 7b) to values well below unity even at scales smaller than 100 m. This velocity-based aspect ratio (23) then decreases much more slowly with horizontal scale beginning at about 100 m. The main exception is the strongest class of bora turbulence where the velocity-based aspect ratio decreases only slowly with scale even at small scales, implying limited influence of stability for the observed

range of scales. The spectral version of (23) shows similar behavior. In summary, the stability influence at the smallest scales increases rapidly with scale leading to suppression of vertical motion and decrease of the velocity aspect ratio. This effect is, of course, most dramatic with the classes of strong stratification and weak turbulence.

c. *Intermittency*

Intermittency and dissipation of kinetic energy are important features of turbulence which can be related to the statistics of velocity gradients (Townsend, 1976). Here, intermittency is posed in terms of the structure function kurtosis or flatness factor (Orszag, 1977; Antonia and Van Atta, 1978):

$$K(r) = [\{\phi(x+r) - \phi(x)\}^4]/[\{\phi(x+r) - \phi(x)\}^2]^2,$$

where the square brackets again indicate simple unweighted averaging. Significant kurtosis is generated not only by spatial variations of turbulence activity, but also by the sharp boundaries of the more vigorous events.

The largest kurtosis for vertical velocity occurs for the classes of weakest turbulence (Fig. 8). The kurtosis is especially large at small scales for the weakest class of nocturnal boundary layer turbulence where intermittency is most obvious from visual inspection of the records. Here patches of turbulence occur separated by regions of little turbulence activity. The bora class of weak turbulence contains both cases of intermittent turbulence with large kurtosis and cases of very weak, perhaps decaying turbulence, with no sharp gradients and smaller kurtosis. However, only for the class of strong nocturnal boundary layer turbulence does the kurtosis approach the Gaussian value of 3.

The decrease of the kurtosis with increasing strength of turbulence is opposite to the case of low Reynolds number flow where the kurtosis and intermittency increase with turbulence strength. In low Reynolds number flows, intermittency is constrained by the influence of viscosity and patches of significant turbulence develop only with a sufficiently high Reynolds number. In the present case where the Reynolds number is not a controlling factor for the main eddies, large intermittency is due more to local suppression of turbulence by stratification and the kurtosis decreases when turbulence is allowed to remain strong everywhere.

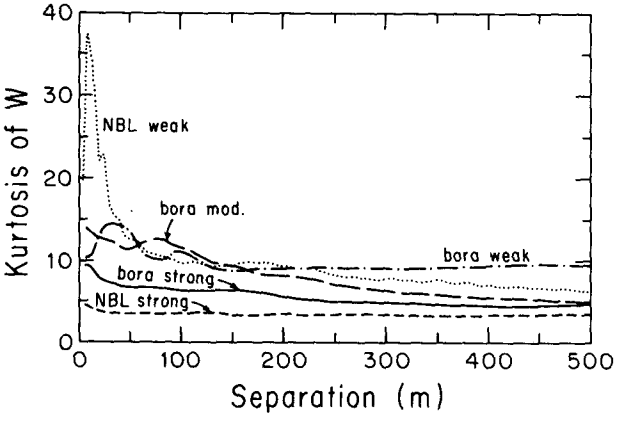

FIG. 8. Composited kurtosis for the structure function for records in the ALPEX bora with strong turbulence (solid), moderate turbulence (broken), and weak turbulence (dash dot), and for the SESAME nocturnal boundary layer case of weak turbulence (dotted) and stronger turbulence (short dash).

d. *Scale regimes*

The foregoing results indicate that the dependence of the spectra and various structure functions on scale can be divided into several subranges. While no classification scheme can adequately describe all of the situations, we have sketched idealized scale regimes in Fig. 9 in order to help organize the statistical claims of this section. When differences arise, the construction of the scale regimes in Fig. 9 for the case of strong turbulence is based more on the bora flow while the weak turbulence case emphasizes the nocturnal boundary-layer case. Figure 9 summarizes the fact that structure and spectral slopes at small scales are smaller for weak turbulence and yield to other influences at smaller horizontal scales. We have also included the general trend that at the smallest scales for weak turbulence, both the structure skewness (see section 5) and the kurtosis are often quite large at approximately the same scales where the buoyancy length increases rapidly and the velocity aspect ratio decreases rapidly with increasing horizontal scale.

5. Types of turbulence

The analyses in section 4 examined the dependence of statistical properties on stability and horizontal scale. In this section, we examine features of the turbulence which appear to be determined by other factors, such as the "age" of the turbulence.

a. *Relationships between characteristics*

To indicate some of the differences between individual turbulence records, statistics for 200 m separation distance are displayed in Figs. 10–11. It must be remembered that individual record sections are more vulnerable to sampling problems compared to the statistics for an entire class of records. In Figs. 10–11, results are plotted in terms of the buoyancy length to estimate the dependence on stability. The velocity aspect ratio tends to decrease with decreasing buoyancy length (increasing stability) and large values of the kurtosis and implied intermittency occur with small buoyancy length (Figs. 10–11). Both tendencies are consistent with the expected constraining influence of

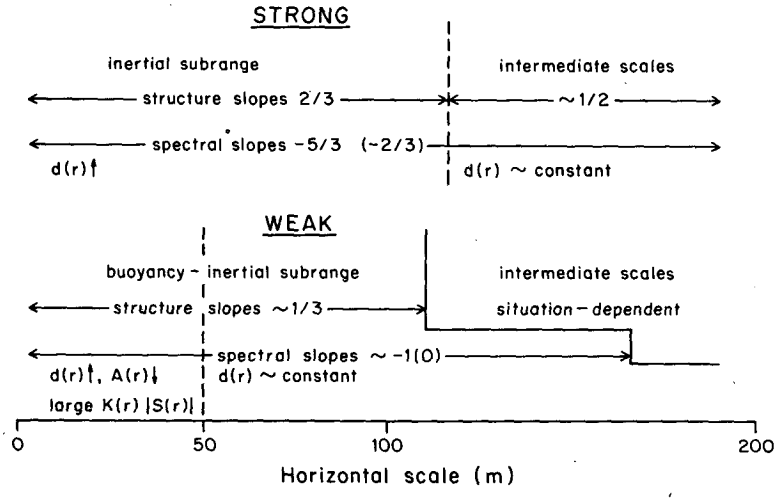

FIG. 9. Schematic depiction of scale regimes for weak or partially suppressed turbulence and strong turbulence. The upward-pointing arrow indicates rapid increase with horizontal scale, $d(r)$ is the buoyancy length, $S(r)$ the skewness and $K(r)$ the kurtosis. Slopes for power spectra of vertical motion are indicated; slopes for $\ln[kE(k)]$ vs $\ln k$ coordinates are in parentheses. See text for further explanation.

stability on the turbulence. These tendencies are clearest when considering different records for a given day.

The relationships between the buoyancy length, velocity aspect ratio and higher moment statistics also indicate the importance of other factors. For example, the bora upstream zone of intermittent turbulence exhibits especially large kurtosis for a variety of turbulence strengths. The strong turbulence in the nocturnal boundary layer is characterized by smaller kurtosis and smaller velocity–aspect ratio relative to the bora turbulence for the same values of buoyancy length and turbulence strength. Apparently the influence of the ground leads to more continuous turbulence but dynamically constrains the vertical velocities more than in the elevated bora turbulence.

b. *Asymmetry of drafts*

Distinct types of turbulence are revealed by examining the variation of the structure skewness defined as

$$S(r) = [\{\phi(x+r) - \phi(x)\}^3]/[\{\phi(x+r) - \phi(x)\}^2]^{3/2}. \quad (24)$$

The magnitude of the structure skewness can be interpreted in terms of general anisotropy and intermittency while the sign of the structure skewness indicates systematic asymmetry of the motions with respect to the mean shear.

The sign of the skewness for vertical motion can be interpreted in terms of two plausible regimes (Fig. 12).

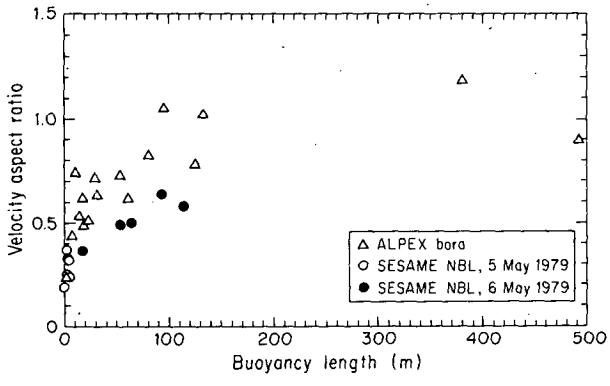

FIG. 10. Velocity aspect ratio [Eq. (23)] as a function of buoyancy length [Eq. (21)] for a separation distance of 200 m for the individual records in the ALPEX bora (triangle), and SESAME nocturnal boundary layer cases of weak turbulence (open circle), and strong turbulence (solid circle).

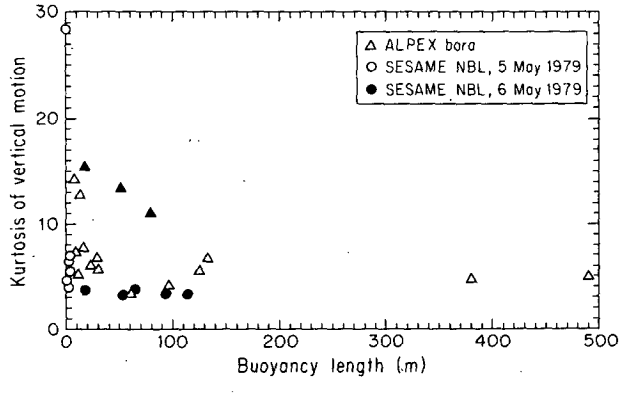

FIG. 11. Structure kurtosis vs buoyancy length for a separation distance of 200 m for the ALPEX bora (triangle) and SESAME nocturnal boundary layer cases of weak (open circle) and strong turbulence (solid circles). Solid triangles indicate the record segments in the upstream bora region of intermittent turbulence (see Fig. 3; segments V1, W1, X2).

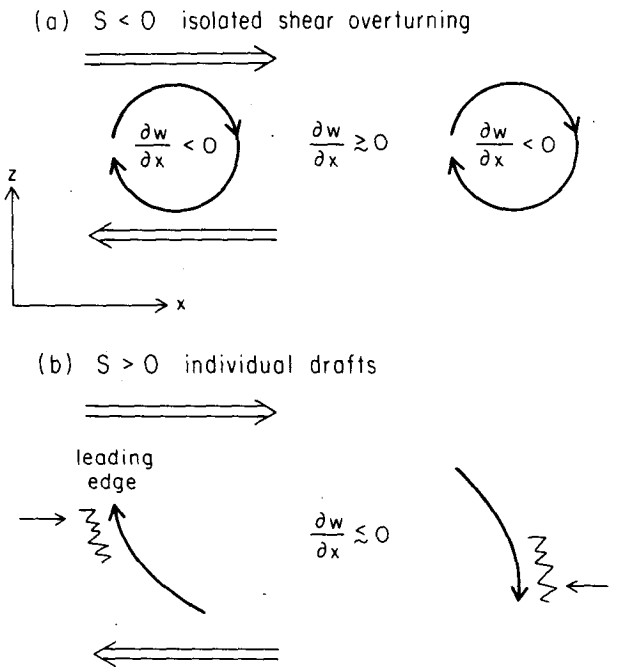

FIG. 12. Idealized models for (a) negative structure skewness due to isolated events of shear-generated overturning and (b) positive structure skewness with individual updrafts and downdrafts. The ragged line indicates the leading edge of the draft characterized by sharp gradients (large positive values of $\partial w/\partial x$). The mean wind vectors (double arrows) are plotted to indicate the bulk shear direction.

If the turbulence is characterized by intermittent overturning events, then the updrafts and downdrafts occur in pairs with larger intervening regions of less activity. For the case sketched in Fig. 12, negative horizontal gradients of vertical motion would occur in the regions of overturning. In the regions between events, the gradient is positive but too weak to contribute significantly to the skewness so that the overall skewness is negative.

If the turbulence is continuous, then the relative horizontal velocity of the updraft or downdraft dictated by the mean vertical shear may become more important as in the example in Fig. 12b. Although the momentum of drafts is not completely conserved because of small-scale mixing and pressure effects, the vertical mean shear normally leads to relative horizontal motions corresponding to momentum transport.

As a result of this relative motion, the draft may be characterized by a sharply defined leading edge, or eddy microfront, where the flow is horizontally convergent and a diffuse trailing edge associated with a downstream wake as noted in Figure 12b. Similar shear-induced asymmetry is observed with boundary layer thermals (Kaimal and Businger, 1970) and boundary layer penetrative convection (Mahrt, 1981). Asymmetric structure seems to be particularly prevalent near solid boundaries (e.g., Blackwelder and Kaplan, 1976; Subramanian et al., 1982; Schols, 1984). The asymmetry is often described in terms of temperature ramp structures. The horizontal structure of most of the drafts in the turbulence studied here are better described by asymmetric top hats although shapes similar to ramps and symmetric top hats also occur.

At the leading edge of the drafts where a sharp microfront is expected, large positive horizontal gradients of vertical motion are generated as sketched in the second example of Fig. 12. These positive gradients contribute more to the structure skewness of the vertical motion than the weaker negative horizontal gradients even if the latter occurs over a greater area. As a result the overall skewness is expected to be positive. If the drafts are viewed as occurring in pairs as a part of an eddy overturning motion, then the region of strong gradients coincide with the edge of the eddy (e.g., Gibson et al., 1968; Brown and Thomas, 1977; Laufer, 1975).

Posed in terms of the coordinate convention in Fig. 12, the nocturnal boundary layer class of weak turbulence is characterized by significant negative skewness, averaging about −0.2 on scales less than 300 m. The negative values are consistent with the occurrence of intermittent turbulence as interpreted in the first example of Fig. 12. The class of weak bora turbulence is also characterized by negative skewness averaging about −0.3 for scales less than 500 m.

In contrast, in the bora flow class of strong turbulence, the skewness in the coordinate system of Fig. 12 is about 0.3, consistent with the sign of the model of microfronts (Fig. 12b). In the example of strongest turbulence at the lowest flight level (Fig. 4), one notices that updrafts are generally characterized by concentrated horizontal gradients of vertical motion on the right boundaries while the changes on the left boundaries are usually more diffuse although this asymmetry is not as pronounced as in some examples in the atmospheric surface layer. Noting that the direction of the local shear for Fig. 4 is to the left, the skewness of the vertical velocity structure for this motion is positive in the coordinate system of Fig. 12 and, therefore, consistent with the model of eddy microfronts (Fig. 12b). This conclusion is tentative since the vertical mean shear is noisy and depends on vertical scale (Figs. 3 and 15). The values of the buoyancy length (Fig. 7a) suggests that within the vertical resolution of the data, the local shear between adjacent levels is most relevant.

Individual records in the bora intermediate class again show considerable spatial variation. Turbulence immediately above the mountain range shows expected large negative skewness as well as large kurtosis especially at the smallest resolvable scales. These statistics suggest intermittent generation of turbulence. In the turbulence immediately "downstream" from the coastal range, the kurtosis is not so large but still reaches maximum values at scales of 50 m or less. Here the turbulence is more continuous. Still farther downstream, where the turbulence is possibly in a stage of decay, the kurtosis is small with maximum values at

relatively large scales. Here sharp gradients are no longer maintained.

c. *Turbulence regimes*

The aforementioned analyses suggest considerable spatial variation of the nature of the turbulence in the bora flow and variation between nocturnal boundary layers. In an attempt to summarize the above results, we define three turbulence regimes which are not complete but help to organize the previous statistical findings. In the first regime, turbulence is intermittently generated by shear as in the nocturnal boundary-layer case of weak turbulence and also in the developing bora turbulence above the mountain ridge. This turbulence is mixed with significant gravity wave activity. The upstream bora turbulence falls into the class of moderate turbulence strength but is qualitatively quite different from the moderate turbulence further downstream.

In the second regime, the turbulence is quite strong including vigorous drafts. The drafts are characterized by sharp boundaries, particularly on their upstream edges where the relative horizontal motion of the draft leads to convergence. These drafts generally lead to downward heat transport. This regime describes the strongest bora turbulence immediately downstream from the mountain crest.

Turbulence in the third regime is continuous but not as strong and contains neither vigorous well-defined drafts nor large skewness. This regime describes the moderate and weak turbulence farther downstream in the bora and broadly describes the strong case of nocturnal boundary layer turbulence. Approximate locations of the different types of turbulence in the bora are noted in Fig. 13.

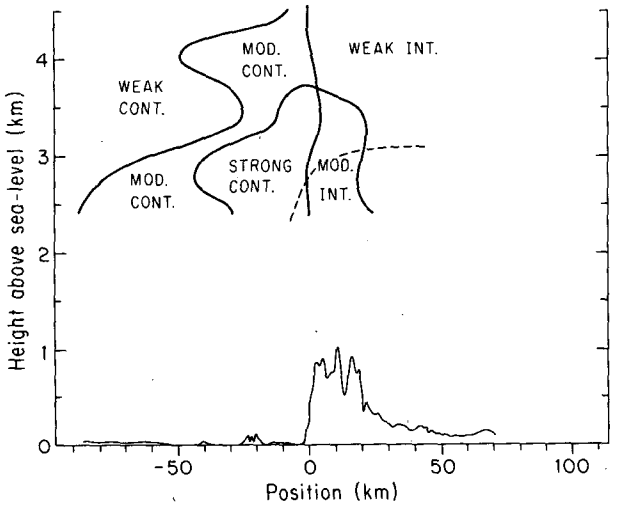

FIG. 13. Plausible spatial partitioning of turbulence regimes in the ALPEX bora based on the classifications of strong, moderate (mod.) and weak turbulence and the distinction between continuous (cont.) or intermittent (int.) turbulence.

6. Costructure

In this section, we study the costructure as a function of horizontal scale in an effort to establish some information on the structure of "statistical eddies". The study of the cospectra would be preferable since they represent orthogonal decomposition of the flux. However, after the needed smoothing to reduce the noise, the property of orthogonal decomposition is lost and the results look rather like the costructure.

The costructure functions for the nocturnal boundary layer are generally consistent with fluctuations predicted by gradient vertical transfer. However, in the bora flow, the costructure functions for vertical motion and the horizontal velocity components are sometimes counter to the gradient as inferred from the general direction of the local shear.

The difference between bora turbulence and nocturnal boundary layer turbulence is also revealed by the examination of the costructure between the horizontal wind components

$$D_{uv}(r) = [\{u(x+r) - u(x)\}\{v(x+r) - v(x)\}]. \quad (25)$$

Only part of the behavior of this costructure function can be explained by the direction of the mean shear. Turbulence fluctuations are generated in the horizontal direction of the mean shear by shear instability. Kinetic energy is generated in the other horizontal direction through secondary three-dimensional instabilities (e.g., Corcos and Lin, 1984) and development of longitudinal modes (Pierrehumbert and Widnall, 1982). In the absence of domination by longitudinal modes, one normally expects the horizontal velocity fluctuations to be largest in the direction of the mean shear, at least on the scale of the energy containing eddies where the shear generation of turbulence is greatest.

The composited costructure for the horizontal velocity components expressed in normal meteorological coordinates is shown in Figure 14. In the nocturnal boundary-layer case of weak turbulence, the mean shear is directed northwestward which causes (Fig. 14)

$$D_{uv}(r) < 0.$$

For the nocturnal boundary-layer case of strong turbulence, the shear is directed northeastward causing

$$D_{uv}(r) > 0.$$

In the bora turbulence, the shear is directed mainly between the north and northeast (Figure 15). Local variations of the shear are probably not significant within the accuracy of the analysis; therefore, the shear is expected to generate positive values of $D_{uv}(r)$. However, for the moderate and strong bora turbulence, the costructure for the horizontal velocity components are systematically negative at least for scales up to a few hundred meters as is also evident in the composited costructure (Fig. 14). For the class of weak bora turbulence, the costructure function (25) is small but agrees in sign with the shear direction.

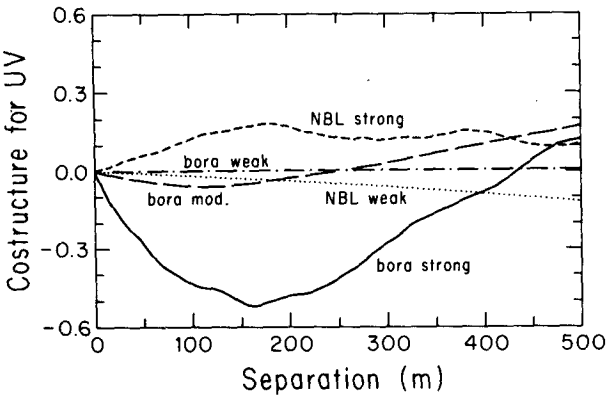

FIG. 14. Composited costructure functions for the horizontal velocity components.

Additional information is revealed by searching for the maximum value of the ratio

$$D_{vv}(r)/D_{uu}(r) \qquad (26)$$

for a given value of r for different rotations of the x–y coordinates about the vertical axis. In this manner, the direction of maximum horizontal velocity fluctuations can be found. As an example, the direction of maximum values of the ratio (26) for $r = 300$ m are shown in Fig. 15. For the class of strong turbulence, the direction of the maximum value of (26) is about 90° to the left of the direction of the overall shear for three of the four segments while the class of moderate turbulence shows considerable variation. In contrast, the direction of maximum values of (26) for the weak turbulence tends to be more parallel to the mean shear except at the highest levels where the shear is weak.

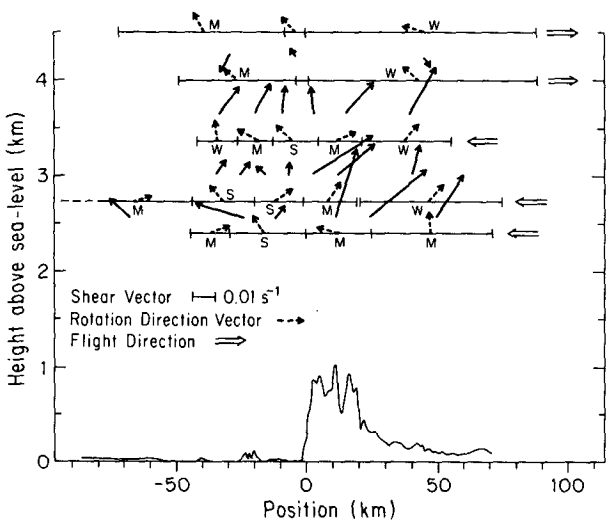

FIG. 15. Cross section of the vertical shear of the horizontal wind vector (solid arrows) and the direction of maximum value of the ratio of the structure functions for the horizontal velocity components (dashed arrows) both plotted in a local planview coordinate system with north directed toward the top of the figure. The cross section itself faces northwestward. See Fig. 3 for further explanation.

The dominance of motion perpendicular to the shear for the strong turbulence could be generated by longitudinal modes which are often observed as rolls in the atmospheric boundary layer (LeMone, 1973) and may occur as pairs of counter-rotating vorticies as with double rollers (Townsend, 1970) and hairpin vorticies (Moin and Kim, 1985). The strong horizontal divergence in the bora flow over the mountain range and in the downstream turbulent region (Fig. 3) would encourage enhancement of vorticity in the flow direction (longitudinal modes) through vortex stretching. A photograph of the bora flow on the following day of 7 March (Fig. 16) indicates considerable organization with axes roughly parallel to the shear vector.

The preferred direction of horizontal velocity fluctuations may also be influenced by the restriction of velocity fluctuations in the flight direction by mass continuity, which in this case would constrain variations parallel to the mean shear more than motions perpendicular to the mean shear. For example, the theory of homogeneous isotropic turbulence (von Karman and Howarth, 1938; Townsend, 1976) predicts the ratio (26) for the inertial subrange to be 4/3 when x is the direction of the sensor motion. The predominance of horizontal motions perpendicular to the shear could also be due to gravity waves with phase lines oriented in the direction of the shear. The problem cannot be resolved with the present data.

7. Conclusions

The structure function possesses advantageous properties for the analysis of motions which are highly nonlinear with no obvious dominate scales or gaps in scales. In particular, the structure function is based on gradients and therefore does not require definition of a local mean and is less vulnerable to trend.

In the present study, spectra and various structure functions were computed from aircraft turbulence data collected in nocturnal boundary layers and collected in turbulence in stratified flow over mountainous terrain. The main conclusions are as follows:

1) The structure buoyancy length is found to be a useful indicator of overall stability in that it does not require computation of vertical gradients and is not sensitive to the choice of horizontal scale.

2) At the smaller horizontal scales, stratification acts to decrease the slope of the spectral energy density and structure functions to values smaller than predicted by inertial subrange theory.

3) The slopes of the spectral density and structure functions at intermediate scales between the inertial subrange and the mesoscale motions appear to be sometimes influenced more by the relative strengths of the turbulence and mesoscale motions than the actual characteristics of the motions at intermediate scales. Similar conclusions are implied by the analysis of Vinnichenko (1970). For example, the slopes at intermediate scales become especially large in situations

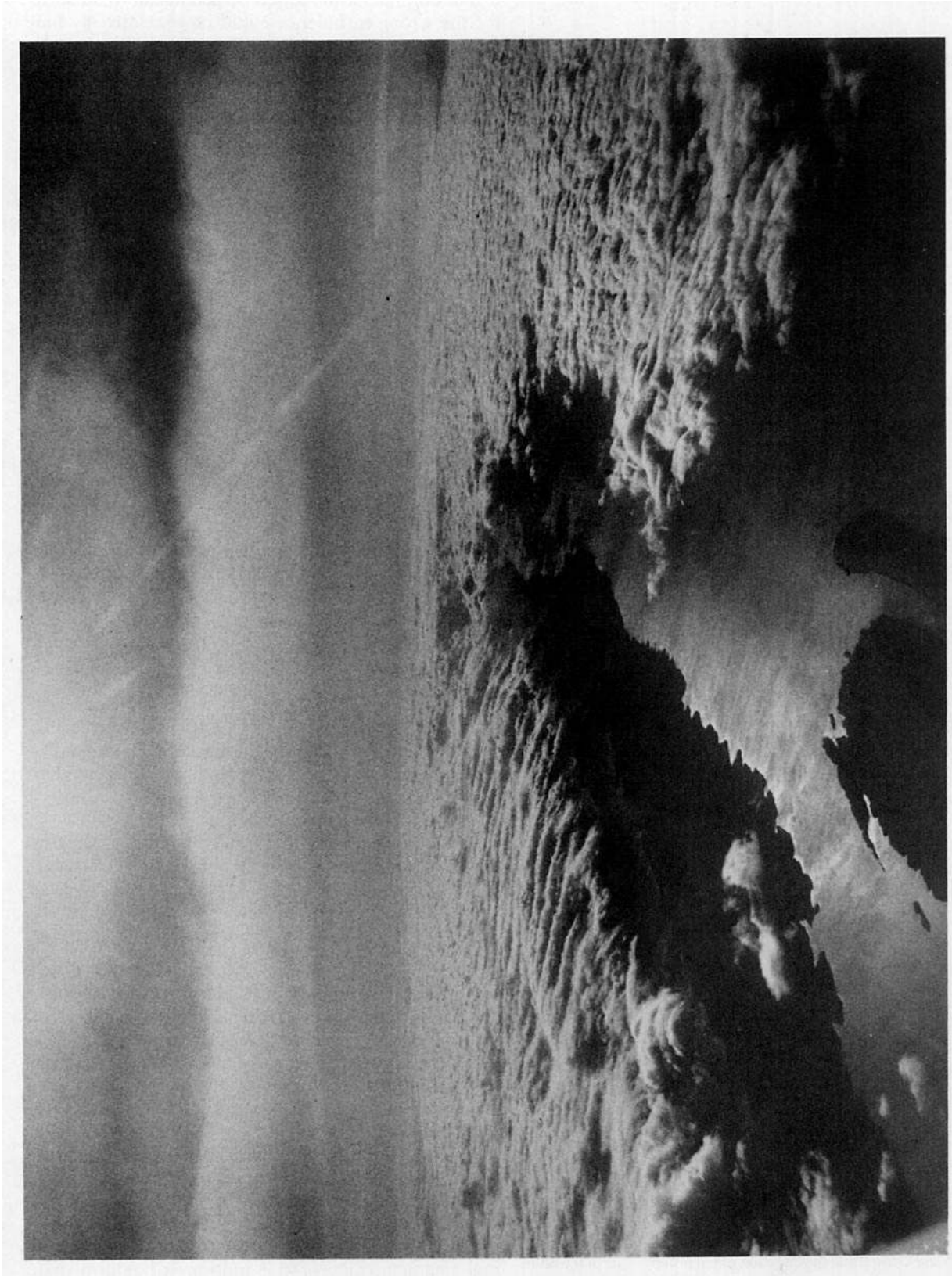

FIG. 16. Photograph of the bora on the following day (7 March 1982) suggesting circulations perpendicular to the flow. (Photograph by Hans Fimpel).

of partially suppressed turbulence and strong mesoscale variance.

4) Turbulence strongly influenced by stratification is characterized by small velocity aspect ratios and often characterized by large structure kurtosis and skewness. The latter are due to significant intermittency. However, in some regions of comparable stability, the weak turbulence is continuous without large kurtosis or skewness and seems to be in a state of decay.

5) The structure skewness for vertical velocity appears to be a useful index which distinguishes intermittent shear-driven overturning from more mature turbulence with strong drafts. The strong drafts are characterized by relative horizontal motion and sharp boundaries particularly on their upstream sides where concentrated gradients can be interpreted as microfronts. The relative horizontal motion of the drafts and horizontal asymmetry is consistent with the expected role of the mean vertical shear.

6) The costructure of the horizontal velocity components in the nocturnal boundary layers agrees with the expected primary generation of the horizontal velocity fluctuations in the direction of the shear. However, the turbulence over the mountainous terrain is more complex and appears to include longitudinal modes.

Acknowledgments. The detailed and valuable comments of Margaret LeMone, Douglas Lilly, and an anonymous reviewer are gratefully acknowledged. Helpful discussions with Helmut Frank, Jelko Urbancic, Donald Lenschow, and Ron Smith and the computational assistance of Wayne Gibson are appreciated. Appreciation is also due to the National Center for Atmospheric Research for computer resources and for use of the Queen Air in SESAME and use of the Electra in ALPEX. The material in this paper is based upon work supported by the Meteorology Program and Global Atmospheric Research Program of the National Science Foundation through grants ATM 8306141 and ATM 8306874.

REFERENCES

Antonia, R. A., and C. W. Van Atta, 1975: On the correlation between temperature and velocity dissipation fields in a heated turbulent jet. *J. Fluid Mech.*, **67**, 273–288.

——, and ——, 1978: Structure functions of temperature fluctuations in turbulent shear flow. *J. Fluid Mech.*, **84**, 561–580.

Babiano, A., C. Basedevant and R. Sodourney, 1985: Structure functions and dispersion laws in two-dimensional turbulence. *J. Atmos. Sci.*, **42**, 941–949.

Blackwelder, R. F., and R. E. Kaplan, 1976: On the wall structure of the turbulent boundary layer. *J. Fluid Mech.*, **76**, 89–112.

Brown, G. L., and A. S. W. Thomas, 1977: Large structure in a turbulent boundary layer. *Phys. Fluids*, **20**(Suppl), 243–252.

Corcos, G. M., and S. J. Lin, 1984: The mixing layer: Deterministic models of a turbulent flow. Part 2. The origin of the three-dimensional motion. *J. Fluid Mech.*, **139**, 67–95.

Finnigan, J. J., F. Einaudi and D. Fua, 1984: The interaction between an internal gravity wave and turbulence in the stably stratified nocturnal boundary layer. *J. Atmos. Sci.*, **41**, 2409–2436.

Gibson, C. H., C. C. Chen and S. C. Lin, 1968: Measurements of turbulent velocity and temperature fluctuations in the wake of a sphere. *AIAA J.*, **6**, 642–649.

Kaimal, J. C., and J. A. Businger, 1970: Case studies of a convective plume and a dust devil. *J. Appl. Meteor.*, **9**, 612–620.

Kolmogorov, A. N., 1941: The local structure of turbulence in incompressible viscous fluid for very large Reynolds numbers. *C. R. Acads. Sci. USSR*, **30**, 301–305.

——, 1962: A refinement of previous hypotheses concerning the local structure in a viscous incompressible fluid at high Reynolds numbers. *J. Fluid Mech.*, **13**, 82–85.

Laufer, J., 1975: New trends in experimental turbulence research. *Annual Review of Fluid Mech.*, **7**, Annual Reviews, 307–326.

LeMone, M. A., 1973: The structure and dynamics of horizontal roll vortices in the planetary boundary layer. *J. Atmos. Sci.*, **30**, 1077–1091.

Lilly, D. K., 1983: Stratified turbulence and the mesoscale variability of the atmosphere. *J. Atmos. Sci.*, **40**, 749–761.

Lumley, J. L., 1964: The spectrum of nearly inertial turbulence in a stably stratified fluid. *J. Atmos. Sci.*, **21**, 99–102.

——, and H. A. Panofsky, 1964: *The Structure of Atmospheric Turbulence*, New York, Interscience, 239 pp.

Mahrt, L., 1981: Circulations in a sheared inversion layer at the mixed layer top. *J. Meterol. Soc. of Japan*, **59**, 238–242.

——, 1985: Vertical structure and turbulence in the very stable boundary layer. *J. Atmos. Sci.*, **42**, 2333–2349.

Moin, P., and J. Kim, 1985: The structure of the vorticity field in turbulent channel flow. Part 1. Analyses of instantaneous fields and statistical correlations. *J. Fluid Mech.*, **155**, 441–464.

Monin, A. S., and A. M. Yaglom, 1975: *Statistical Fluid Mechanics*, **2**, The MIT Press, 873 pp.

Orszag, S. A., 1977: Lectures on the statistical theory of turbulence, *Fluid Dynamics*, R. Balian and J.-L. Paube, eds., Gordin and Breach.

Panofsky, H. A., and J. A. Dutton, 1984: *Atmospheric Turbulence*, John Wiley and Sons, 397 pp.

Pierrehumbert, R. T., and S. E. Widnall, 1982: The two- and three-dimensional instabilities of a spatially periodic shear layer. *J. Fluid Mech.*, **114**, 59–82.

Schols, J. L. J., 1984: The detection and measurement of turbulent structures in the atmospheric surface layer. *Bound.-Layer Meteor.*, **29**, 39–58.

Shur, G. N., 1962: Eksperimental'nyye issledovaniya energeticheskogo spektra atmosfernoy turbulentnosti. Tsentral' naya aerologicheskaya observatoriya. *Trudy*, **43**, 79–90. (Trans. as AID Report T-63-55 Aerospace Info. Div., Lib. Cong.).

Subramanian, C. S., S. Rajagopalan, R. A. Antonia and A. J. Chambers, 1982: Comparison of conditional sampling and averaging techniques in a turbulent boundary layer. *J. Fluid Mech.*, **123**, 335–362.

Tennekes, H., and J. L. Lumley, 1972: *A First Course in Turbulence*, The MIT Press, Cambridge, MA.

Townsend, A. A., 1968: Excitation of internal waves in a stably-stratified atmosphere with considerable wind-shear. *J. Fluid Mech.*, **32**, 145–171.

——, 1970: Entrainment and structure of turbulent shear flow. *J. Fluid Mech.*, **41**, 13–46.

——, 1976: *The Structure of Turbulent Shear Flow*, Cambridge University Press.

Van Atta, C. W., 1971: Influence of fluctuations in local dissipation rates on turbulent scalar characteristics in the inertial subrange. *Phys. Fluids*, **14**, 1803.

Vinnichenko, N. K., 1970: The kinetic energy spectrum in the free atmosphere 1 second to 5 years. *Tellus*, **22**, 158–166.

von Karman, T., and L. Howarth, 1938: On the stratified theory of isotropic turbulence. *Proc. Roy. Soc.*, **A164**, 192–215.

Weinstock, J., 1980: A theory of gaps in the turbulence spectra of stably stratified shear flows. *J. Atmos. Sci.*, **37**, 1542–1549.

Wyngaard, J. C., W. T. Pennell, D. H. Lenschow and M. A. LeMone, 1978: The temperature-humidity covariance budget in the convective boundary layer. *J. Atmos. Sci.*, **35**, 47–58.

Yaglom, A. M., 1966: The influence of fluctuations in energy dissipation on the shape of turbulence characteristics in the inertial interval. *Sov. Phys. Dokl.*, **11**, 26.